Journal of Molecular Liquids 376 (2023) 121415

Contents lists available at ScienceDirect

Journal of Molecular Liquids

journal homepage: www.elsevier.com/locate/molliq

Improving the efficiency of the concentrating solar power plants using heat transfer nanofluids with gold nanoplates: An analysis from laboratory to industrial scale

Iván Carrillo-Berdugo *, Javier Sampalo-Guzmán, Juan Jesús Gallardo, Alejandro Domínguez-Núñez, Teresa Aguilar, Paloma Martínez-Merino, Javier Navas

Departamento de Química Física, Facultad de Ciencias, Universidad de Cádiz, E-11510 Puerto Real (Cádiz), Spain

ARTICLE INFO

Article history:
Received 16 November 2022
Revised 2 February 2023
Accepted 6 February 2023
Available online 7 February 2023

Keywords:
Concentrating solar power
Parabolic trough collectors
Heat transfer fluid
Nanofluids
Thermal properties

ABSTRACT

We report about the remarkable changes in the thermophysical properties of the heat transfer fluid used in concentrating solar power plants with parabolic-trough collectors (Dowtherm A, a mixture of diphenyl oxide and biphenyl) by addition of Au nanoplates in mass fractions around 10^{-2} wt%. The resulting nanofluids are stable for weeks, and their enhanced physical properties make them good candidates for the application. Particularly, with $4.8{\cdot}10^{-2}$ wt% of Au nanoplates, specific heat increases by 12.0 ± 1.2 % at 523 K and thermal conductivity increases by 24.9 ± 6.1 % at 373 K, with no measurable changes in density or dynamic viscosity. This set of physical properties allows to make a realistic estimation of the performance of a prototypical concentrating solar power plant using these nanofluids for solar-to-thermal energy conversion. We determine, using computational cost-free numerical models available in literature, that the performance of a concentrating solar power plant could increase up to 35.1 %, compared to the predicted 24.7 % with the conventional heat transfer fluid, with neither rheological penalties nor economically prohibitive structural changes. The findings here reported may contribute to encourage the application of heat transfer nanofluids in order to improve the efficiency of concentrating solar power plants, and to consolidate a working scheme that positively promotes the transition from laboratory scale to industrial scale.

1. Introduction

We are facing a global climate crisis driven by the indiscriminate emission of CO_2 associated to human activity in general and, in particular, to the electricity production. In the European Union, electricity production accounts for one-third of the emissions from the energy sector, which is responsible of nearly 90 % of the total CO_2 emissions [1], a direct consequence of the strong dependence of this sector on fossil fuels. The situation is further strengthened by rising production costs due to the increasing uncertainty in the availability of fossil fuels [2]. It all evidences the unsustainability of the current scenario and the need for synergic renewable technologies to consolidate a new-generation electricity market. In this sense, concentrating solar power (CSP) technologies, especially when coupled to thermal energy storage (TES) blocks [3], could become a choice for reliable and dispatchable (on-demand) electricity production [4], if it were not for their cost-efficiency. Parabolic trough collectors (PTC) are the most mature arrangement for mirrors in CSP [5,6]. The heat transfer fluid (HTF) of choice in CSP-PTC plants is the eutectic and azeotropic mixture of diphenyl ether (73.5 %) and biphenyl (26.5 %), commercially available as Dowtherm A. It is a suitable HTF for operation in liquid phase at high temperature, for its low vapour pressure (1013 hPa at 530 K) and resistance to thermal decomposition (up to 678 K), low dynamic viscosity (5.00–0.12 mPa·s at 288–678 K) and non-corrosive nature. However, its specific heat (1588–2725 $J{\cdot}kg^{-1}{\cdot}K^{-1}$) and thermal conductivity (0.140–0.077 $W{\cdot}m^{-1}{\cdot}K^{-1}$) are relatively poor compared to the HTFs of choice in other applications, thus limiting the efficiency of the solar-to-thermal-to-electric energy conversion.

The onward advances in the processing of nanomaterials have opened an avenue for the development of a generation of colloids with enhanced thermal properties to be used as HTFs in very demanding energy conversion and thermal management applications: nanofluids [7]. It is proven throughout literature that the dispersion of nanomaterials within conventional fluids affects their specific heat [8,9] and thermal conductivity [10–14], which are

* Corresponding author.
E-mail address: ivan.carrillo@uca.es (I. Carrillo-Berdugo).

https://doi.org/10.1016/j.molliq.2023.121415
0167-7322/

properties of interest for heat transfer [15]. For this, nanofluids can be used in thermal management and energy conversion applications; for instance, in CSP as heat transfer fluids [16]. The idea of using nanofluids for solar-to-thermal energy conversion was first introduced by Tyagi et al. [17] in 2009, who reported on the improved efficiencies of low-temperature nanofluid-based direct absorption solar collectors (DASC). More than two thousand papers on the topic have been published since then. Those focused on large-scale high-temperature photo-thermal conversion are less abundant and mostly published in the second half of the 2012–2021 decade. A part of these studies is devoted to the preparation and characterisation of the thermophysical properties, most notably thermal conductivity, of nanofluids based on synthetic heat transfer oils for high operating temperatures. Singh et al. [18] reported on the viscosity, specific heat and thermal conductivity of Cu nanoparticle-containing nanofluids with the Therminol 59 (alkyl-substituted aromatic compounds) and Therminol 66 (modified terphenyl compounds) as base fluids. They concluded, on the basis of a figure-of-merit (FoM) criterion, that the addition of Cu nanoparticles results into a more significant enhancement for convective heat transfer in the case of Therminol 66. This was the very first report on the development of nanofluids as advanced HTFs using the oils operating in CSP plants as base fluids. An international patent by Juliá et al. [19] introduces a nanofluid consisting of carbon soot particles and diphenyl sulphone in Therminol VP-1 (a HTF with the same composition than the Dowtherm A). They reported an average thermal conductivity enhancement of 15 % for a 5 wt% content of soot. Navas et al. have intensively research Dowtherm A-based heat transfer nanofluids for more efficient CSP plants, covering a wide variety of nanomaterials, including: TiO_2 nanoparticles (14 %, 0.2 vol%) [9], MoS_2 nanosheets (39 %, 0.3 vol%) [20], $MoSe_2$ nanosheets (11 %, 0.1 vol%) [21], WS_2 nanosheets (22 %, $7.5{\cdot}10^{-2}$ vol%) [22], WSe_2 nanosheets (26 %, 0.1 wt%) [23], NiO nanoparticles (50 %, $1.0{\cdot}10^{-4}$ wt%) [24], Pt nanoparticles (20 %, $5.0{\cdot}10^{-3}$ wt%) [25], Ag nanoparticles (6 %, $5.0{\cdot}10^{-4}$ wt%) [12], Au nanoparticles (37 %, 1.6 vol%) [13], BN nanotubes (18 %, 8.6 vol%) [26], and graphene oxide (30 %, 2.0 vol%) [27]. The maximum enhancements in the heat transfer coefficient according to the Dittus-Boelter FoM at 363 K and the mass or volume fractions of nanomaterial are indicated between brackets. Some of these nanofluids where also reported to be excellent candidates for volumetric (direct) absorption [23,27]. Jeong et al. recently reported on very stable Therminol VP-1-based nanofluids based with graphite nanopowders, which exhibit very good photothermal activity [28].

Another part of the studies focusing on nanofluids for solar energy conversion systems is devoted to the assessments of their thermal efficiency, viability, and requirements by means of numerical methods and computational fluid dynamics (CFD). Mwesigye et al. [29–31] investigated the thermodynamic performance PTC using Syltherm 800-based nanofluids with Al_2O_3 nanoparticles and Therminol VP-1-based nanofluids with Cu nanoparticles and single-walled carbon nanotubes (SWCNT). They reported, on the basis of ray tracing-assisted CFD simulations, maximum thermal efficiencies of 77 % (8 vol% Al_2O_3), 74 % (6 vol% Cu) and 73 % (2.5 vol% SWCNT), using nanofluids with an inlet temperature of 400 K and Reynolds number well below 10^5, which are better than the maximum thermal efficiency of 69 % and 71 % using the Syltherm 800 and Therminol VP-1 fluids under the same conditions. Although CFD simulations are a powerful tool for such assessments, these require significant allocation of resources in high-performance computing services to reach results within a reasonable time scale. For that, other works like those of Lenert et al. [32], related to selection criteria of HTF for CSP systems, and Bellos et al. [33], related to the temperature profile and efficiency of PTC collectors in CSP systems, are worth of mention because they provide a computationally inexpensive way to estimate HTF performances and PTC thermal efficiencies that is accessible for routine, as it will be later proven in this work.

Overall, the reviewed literature endorses the use of nanofluids as heat transfer fluids and makes clear that CSP-PTC systems can benefit from it to achieve better yields in solar-to-thermal energy conversion. It also evidences the need for more research, particularly multidisciplinary research, so that the physical properties of the HTF of choice are characterised in presence of a plethora of different nanomaterials and the implications of its their use in the thermal efficiency of the application are fully assessed.

Here, we report on the applicability of Au nanoplate-containing nanofluids for CSP-PTC plants. Nanofluid samples have been prepared following a two-step procedure in which Au nanoplates are first synthesised in a kinetically controlled hydrothermal process and then isolated and dispersed into the Dowtherm A HTF. The colloidal stability and the physical properties of all samples have been characterised to assess their performance as HTF in the application of interest. The assessment considers a two-level approach: (i) using a FoM, as a straightforward indicator for the quantification of the enhancements in heat transfer with respect to the base fluid, and (ii) using an approximate analytic model for the one-dimensional, steady state heat transfer problem under turbulent flow regime for a prediction of the temperature profile of HTFs as they flow through the PTCs. Our work is not methodological with respect to the development of these two approaches but benefits from them to contextualize the results from this study and to rationally assess how much this renewable technology benefits from the use of these nanofluids. It all provides a big picture of the applicability of these nanofluids and lead the way for their transition from basic research at laboratory scale to actual implementation at industrial scale.

2. Methodology

2.1. Synthesis and characterisation of Au nanoplates

The nanoplate shape of face-centred cubic metal nanocrystals, even if it maximises the expression of (1 1 1) facets, is not favoured by thermodynamics because of crystalline lattice strain [34]. For such a shape to be preferentially obtained, the kinetics of nucleation and growth must be exhaustively controlled by slowing down the rates of reduction of the metal precursor. For the shape-controlled synthesis of Au nanoplates, 75.2 mg of $HAuCl_4{\cdot}3H_2O$ (Sigma-Aldrich, 99.9 %) and 542.0 mg of polyvinyl pyrrolidone (Sigma-Aldrich, ave. mol. wt. 40 kDa) were simultaneously added to a round-bottom flask with 11.0 ml of a 10^{-3} M solution of KCl (Sigma-Aldrich) in deionised water. The molar ratio between the Au^{3+} cation and the PVP monomer is 1:25, and the molar ratio between the Au^{3+} cation and the Cl^- anion 1:5. This solution was stirred at 300 rpm for 24 h at room temperature under air atmosphere, for the nanoplates to be formed. Here PVP acts as mild reductor, as the terminal hydroxyl groups are susceptible of oxidation to carboxyl groups, and also as stabiliser, for the steric hindrance imposed by the long-chained carbon-based structure [35]. Alternatively, the Cl^- anions act as stabilisers only, by preferential adsorption on (1 1 1) surfaces, this inhibiting growth along the ⟨1 1 1⟩ direction and promoting growth in perpendicular directions, which leads to the formation of the desired nanoplate morphology [36].

The product was isolated by washing twice with ethanol and once with acetone after successive centrifugations for 15 min at 10000 rpm, to be finally collected in powder form after drying it in vacuum at 333 K for 48 h. Morphology and size distribution of the as-synthesised nanostructured powder were determined by

high resolution transmission microscopy (HRTEM) (FEI, Talos F200S). Crystallinity and chemical state bonding of Au in the sample were assessed by X-ray diffraction (XRD) (Bruker, D8 Advance A25 diffractometer, Cu-Kα source, LYNXEYE detector) and X-ray photoelectron spectroscopy (XPS) (Physical Electronics, PHI 5000 VersaProbe II, monochromatic Al-Kα source).

2.2. Preparation and characterisation of Au nanoplate-containing nanofluids

Following a two-step procedure, 51.6 mg of Au nanoplates were dispersed in 100 ml of a 1 wt% solution of Triton X-100 (Panreac) in Dowtherm A (The Dow Chemical Company) by ultrasonication (Sonics&Materials, VCX-500, solid probe, 13 mm tip), with a 2:4 s on:off pulsation at 50 % amplitude, for an elapsed time of 3 h. The Triton X-100 surfactant, according to its technical and safety datasheets, is suitable for the high operating temperatures demanded by the concentrating solar power application, as it has a boiling point over 473 K at 1013 hPa and it is only susceptible to oxidation in presence of O_2. It is proven later in this paper that the chosen mass fraction of this surfactant does not cause a measurable change in any of the physical properties that define the convection heat transfer coefficient. The colloid resulting from sonication, with a mass fraction of $4.8{\cdot}10^{-2}$ wt% in Au nanoplates, and its 1:2 and 1:5 dilutions, with mass fractions of $2.4{\cdot}10^{-2}$ wt% and $9.7{\cdot}10^{-3}$ wt%, are the nanofluids to be characterised. Samples with different concentrations are under consideration to assess that we are indeed operating within the very dilute regime, as there are previous studies in which the properties of interest are reported not to improve with increasing loadings of nanomaterial beyond a certain limit [37,38]. It is verified throughout the discussion of results that the above stated mass fractions are practically in such regime.

Colloidal stability was first determined in terms of spectral extinction, measured by visible spectroscopy (OceanOptics, DH-2000-BAL light source and USB2000 + general purpose spectrometer), and particle size distribution in suspension, estimated by dynamic light scattering (DLS) (Malvern Instruments, Zetasizer Nano ZS). Both were measured in triplicate over the course of three weeks. Once the time frame for colloidal metastability is determined, the key physical properties for heat transfer and storage (*i.e.*, density, surface tension, dynamic viscosity, specific heat, and thermal conductivity), of the base fluid, the host fluid and all nanofluid samples, were characterised. Density was measured using a vibrating U-shaped tube densitometer (Anton Paar, DM35), at 298 K. Surface tension was measured using an optical contact angle measuring (OCA) and shape analysis system (Dataphysics, OCA 25, needle $Ø_{out}$ = 0.65 mm), following the pendant drop method based on the Young-Laplace equation, at 298 K. The dynamic viscosity and flow behaviour were determined using a rheometer (TA Instruments, Discovery HR 10, concentric cylinder geometry, $Ø_{rotor}$ = 14.0-mm, $Ø_{cup}$ = 15.2 mm), under steady-state shear rate-controlled conditions, within the 1–100 s^{-1} shear rate range. Rheological measurements were performed at 298 K, 323 K, 348 K and 373 K, using an electrically heated concentric jacket for temperature control. Isobaric specific heat was determined by differential scanning calorimetry (DSC) (Netzsch, DSC 214 Polyma, closed concavus pan), setting a temperature-modulated dynamic program from 293 K to 528 K at 1 $K{\cdot}min^{-1}$ with a modulation of ± 1 K in amplitude and 120 s in periodicity. Specific heat was calculated using the ratio method, for which the DSC signal baseline was corrected and compared to the DSC signal from a sapphire certificated reference sample, using the same temperature program. Thermal conductivity was measured using the transient hot-bridge technique with a hot point sensor (THB-HPS) (Linseis, THB-100, sensor type C), with a measurement time of 10 s for an input power of 32 mW, with a delay of 30 s between replicas. Liquid samples were contained in cylindrical glass vials, with 2.5 ml of capacity, and hold in individually jacketed vessels in a dry block heater (IKA, DB 5.2) at 298 K, 323 K, 348 K and 373 K. All measurements were performed in triplicate for each sample and temperature, except for THB-HPS measurements, for which ten replicas were recorded for each case Fig. 1.

3. Results and discussion

3.1. Structural and compositional characterisation of Au nanoplates

An exhaustive structural and compositional characterisation of the product of synthesis was undertaken to verify the successful obtention of the desired Au nanoplates before dispersion in the base fluid. TEM images of Au nanoplates are presented in Fig. 2A-C. The prevalence of the nanoplate morphology in the product is about 30 %, a regular percentage for these kind of synthetic procedures [36]. Nanoplates have truncated-corner triangular and hexagonal contours, and the electron transparency, recognisable in most cases, suggests these are 2D nanostructures. The lateral size is within 200–800 nm, although larger nanoplates, like the one in Fig. 2C (about 3 μm), are also found.

The powder diffractogram in Fig. 2D makes clear that the Bragg condition for maximum diffracted intensity is fulfilled for 2θ equal to 38.2°, 44.4°, 64.6°, 77.6° and 81.7°, a pattern that matches the expected angles for the diffraction from (111), (200), (220), (311) and (222) planes of fcc Au. Finally, the formal oxidation state of Au was also verified by XPS. The general survey spectrum is available in Fig. 2E. All signals are conveniently referenced to the C 1 s transition, at 284.8 eV, assigned to adventitious carbon. The Au 4f signal, shown in Fig. 2F with high resolution, is the primary region for the assignment of Au metal. Here two-well defined spin–orbit components can be identified, Au $4f_{7/2}$ and Au $4f_{5/2}$, at 84.1 eV and 87.8 eV. A binding energy of 84.1 eV for Au $4f_{7/2}$, a chemical shift of 3.7 eV between spin–orbit split peaks in this region and asymmetric peak shapes are sufficient to determine that the chemical state of the as-synthesised sample is Au metal [39].

3.2. Colloidal stability of Au nanoplate-containing nanofluids

The applicability of these nanofluids as working fluids, for any application, is subjected to its colloidal stability. Disperse phases are thermodynamically prone to aggregation, as it minimises the interfacial area and so the surface free energy of the colloid (metallic nanomaterials, for instance, have an enormous surface tension). That implies a loss of availability of monodisperse nanoparticles in suspension, and so of any potential enhancement in thermal conductivity or specific heat, which is ultimately translated into a loss of its operational value. Aggregation is a thermodynamically spontaneous process that minimises surface free energy. Metals in particular, as it is the case under study, have very high surface free energy due to the strong (metallic) chemical bonding between their atoms. Aggregation can only be temporarily impeded by slowing down the kinetics of the process via electrosteric repulsions between particles in suspension, thus leading to a metastable situation. Ensuring such a situation is a *sine qua non* condition for a reliable determination of the changes in thermal and rheological properties of nanofluids with respect to their base fluid. For that, in the sonication-assisted dispersion of Au nanoplates, 1 wt% of the Triton X-100 surfactant was added to the Dowtherm A base fluid. Its functionality is to be proven.

Goodness criteria for colloidal stability demands minimum variation in the load of nanomaterial in suspension over a wide time window. This was monitored by analysing the time-

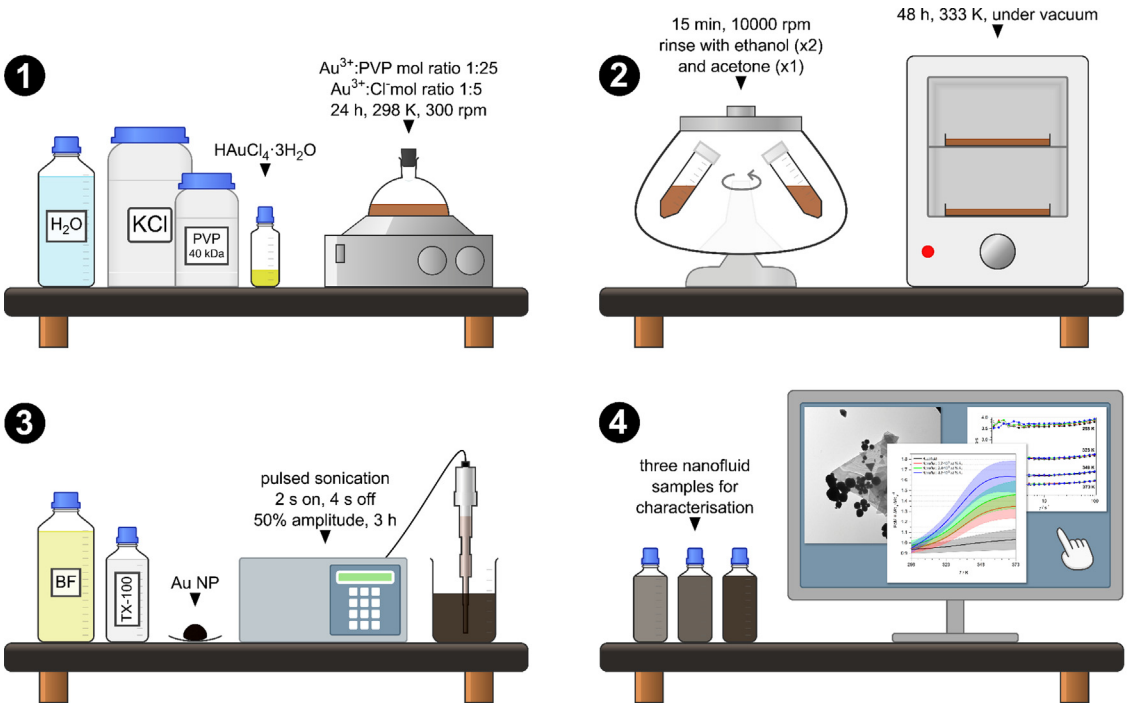

Fig. 1. Summary of the experimental procedure around Au nanoplate-containing nanofluids: (1) synthesis of the nanomaterial, (2) isolation of the nanomaterial, (3) preparation of nanofluids and (4) characterisation of the nanomaterial and the nanofluids.

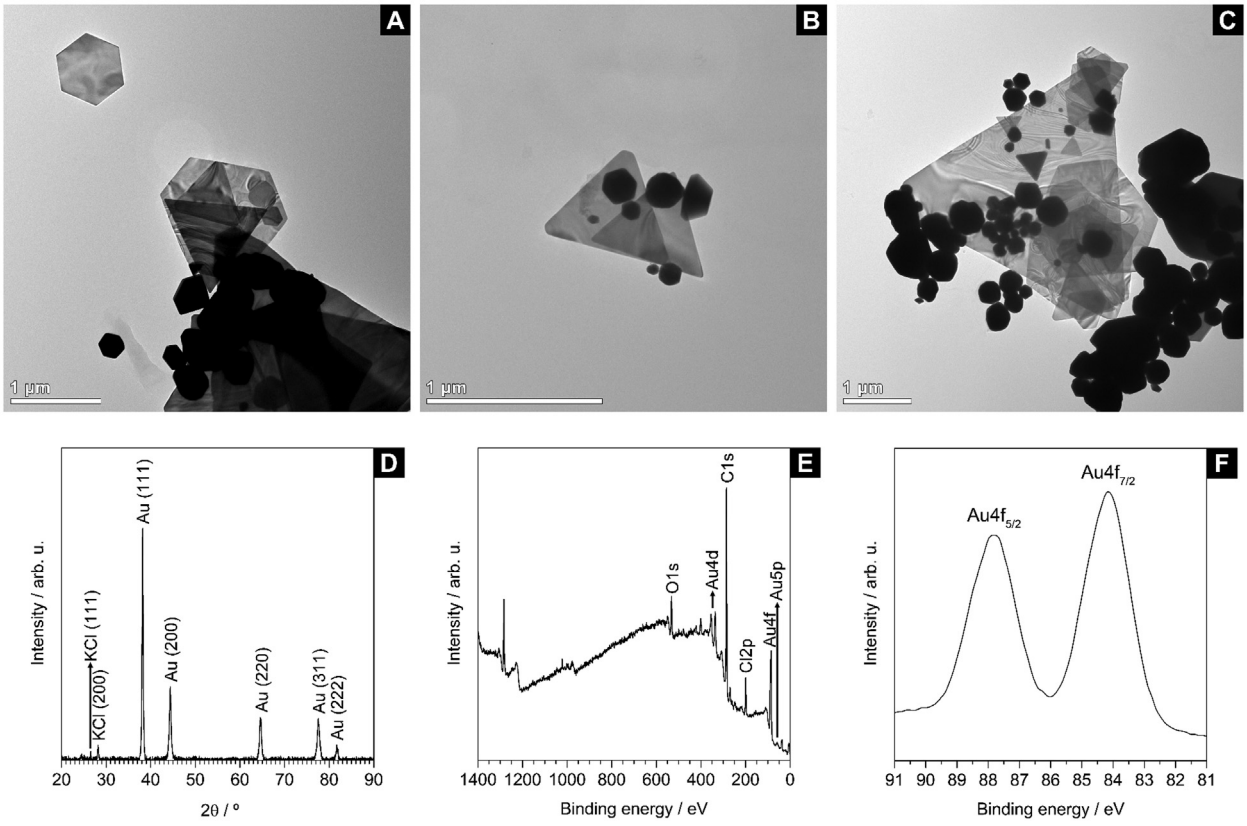

Fig. 2. Structural and compositional characterisation of Au nanoplates: typical TEM images [A-C], powder X-ray diffractogram [D], and X-ray photoelectron spectra for general purpose analysis [E] and high-resolution analysis of the Au 4f region [F].

resolved visible extinction spectra of the $4.8{\cdot}10^{-2}$ wt% (undiluted) Au nanoplate-containing nanofluid sample. The zero-time extinction spectrum, using the base fluid as reference, is presented in the inset of Fig. 3A as an example of the typical spectrum for this sample. Light is extinguished over the entire visible range due to direct absorption of photons, and scattering and secondary absorp-

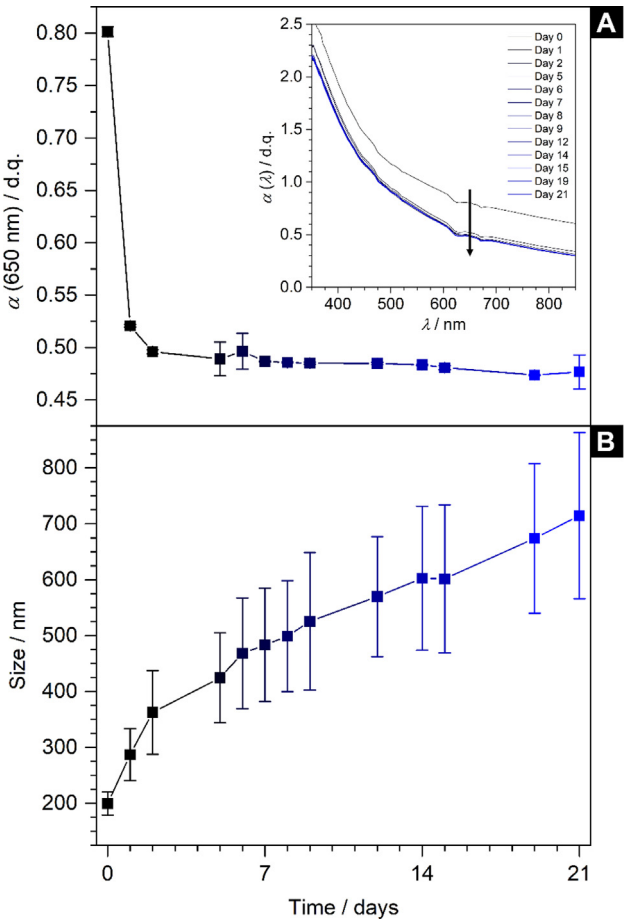

Fig. 3. Colloidal stability indicators for Au nanoplate-containing nanofluids: changes in spectral extinction [A] and particle size distribution [B] over time. Solid lines do not represent actual data but are included as guide to the eye.

tion of photons, which further increases extinction levels. The scattering effect is particularly acute at shorter wavelengths, for which the scattering cross-section is predominant. Absorption is due to the localised surface plasmon resonance of Au nanoplates, which is known to occur in the 400–1200 nm range of wavelengths [40,41], a range sensitive to the lateral size of the nanoplates and the dispersant medium. Although the absorption and scattering components are not differentiated in this study, a unique band in the 620–680 nm range is identified. The time evolution of the extinction value at 650 nm is plotted in Fig. 3A, for a semiquantitative evaluation of the variations in the load of nanoplates in suspension. It decreases by 38 % by the end of the third day after preparation, and remains stable afterwards. Such a decrease is closely related to an aggregation phenomenon, according to Fig. 3B. Size distribution remains monomodal, but its mean and standard deviation increase over time, from 199.4 ± 20.6 nm to 714.8 ± 148.6 nm. The increase in the standard deviation evidences a transition from mesokurtic to platykurtic regime, which is ultimately translated into an increase in dispersity. Overall, proven that spectral extinction remains stable and that no phase segregation or sedimentation occurs during the entire characterisation time window, it is safe to conclude that the nanofluid achieves a metastable situation and that goodness criterion for colloidal stability is fulfilled.

3.3. Physical properties of Au nanoplate-containing nanofluids

Once the applicability has been verified, the effectiveness of these nanofluids as working fluids must be assessed. Most FoM aimed to assess the performance of heat transfer fluids give significance to density ρ, dynamic viscosity η, specific heat c and thermal conductivity κ, as dominant factors affecting the energy storage and transfer processes. Surface tension γ is also considered under certain boundary conditions [42]. For that, we characterised these five physical properties of the base fluid, the host fluid and all nanofluid samples.

Density and surface tension – Density and surface tension values are reported in Table 1. The standard deviation of the density measurements is better than ± 0.01 %. The measured density datum for the base fluid, at 298 K, is known to have a systematic relative deviation below 0.06 % with respect to the reference density datum provided by the supplier at the same temperature (1055.7 kg·m^{-3}), which ratifies the goodness of the measurement. The difference between the density values of the host fluid and the base fluid is not significantly discernible from the standard deviation of the measurements, and the addition of the Triton X-100 surfactant (1.0 wt%) is consequently determined not to cause a measurable change in density. The addition of Au nanoplates causes a measurable yet small increment in density, but the differences between samples are not significantly discernible from the standard deviation of the measurements either. That is an expected situation considering samples are in a very diluted regime, for which such an increment in density is not expected to have a significant impact on convection heat transfer or pressure loss.

Regarding surface tension, the standard deviation of its measurement is better than ± 3.2 %. The measured surface tension datum for the base fluid, at 298 K, is known to have a relative deviation below 6.2 % with respect to the reference surface tension datum provided by the supplier at the same temperature (40.1 mN·m^{-1}), which ratifies the goodness of the measurement. The addition of Triton X-100 in the concentration above stated is determined to increase surface tension by 4.8 ± 3.9 % with respect to the base fluid. The addition of Au nanoplates has a major effect, with increments up to 24.7 ± 2.3 %. Although these nanofluids are involved in boiling heat transfer processes in PTC of CSP plants, this change in surface tension should not be ignored and be expected to be pivotal for other applications, as the boiling heat transfer coefficient in such cases is inversely proportional to surface tension [42], thus having a negative effect.

Dynamic viscosity– The steady-state shear flow behaviour of the samples is discussed based on the dynamic viscosity profiles presented in Fig. 4A, for all samples and temperatures, as a function of the shear rate. The reliable measurement range for the determination of the viscosity [43] of these samples in our rotational rheometer with a concentric cylinder geometry is defined between 5 s^{-1} and 20 s^{-1}. At lower shear rates there are fluctuating viscosity values due to operation in the lower torque detection limit and initial elastic deformation effects. At higher shear rates the flow regime transitions from laminar to turbulent, and vibrations worsen the quality of the measurement by artificially increasing the apparent viscosity due to an increasing bearing friction in the rotor. A clear turbulent flow regime exists for shear rates over 100 s^{-1}, with frequent sample ejection events. All samples exhibit a Newtonian behaviour within that reliable range.

The average viscosity is presented in Fig. 4B, as a function of temperature. The relative standard deviation of the measurements is better than ± 1.4 %. The measured viscosity values for the base fluid are in good agreement compared to the reference viscosity values provided by the supplier, with a maximum relative deviation below 3.3 %. The addition of Triton X-100 (1.0 wt%) is proven not to change the flow behaviour and not to cause a measurable change in viscosity (as for density, the differences are not significantly discernible from the standard deviation of the measurements). This validates our previous statement on the choice of this surfactant, at the given concentration, for decent colloidal stability without rheological penalty. All nanofluid samples preserved

Table 1
Summary of samples and their measured density and surface tension values, at 298 K.

Sample	χ_{TX100}/wt.%	χ_{Au}/wt.%	ρ/ kg·m^{-3}	γ/mN·m^{-1}
Base fluid	0.0	0.0	1056.3 ± 0.1	37.6 ± 0.8
Host fluid	1.0	0.0	1056.4 ± 0.1	39.4 ± 1.2
Nanofluid 1:5	1.0	$9.7{\cdot}10^{-3}$	1056.8 ± 0.1	48.9 ± 0.6
Nanofluid 1:2	1.0	$2.4{\cdot}10^{-2}$	1056.7 ± 0.2	45.7 ± 0.3
Nanofluid 1:1	1.0	$4.8{\cdot}10^{-2}$	1056.9 ± 0.1	47.0 ± 1.0

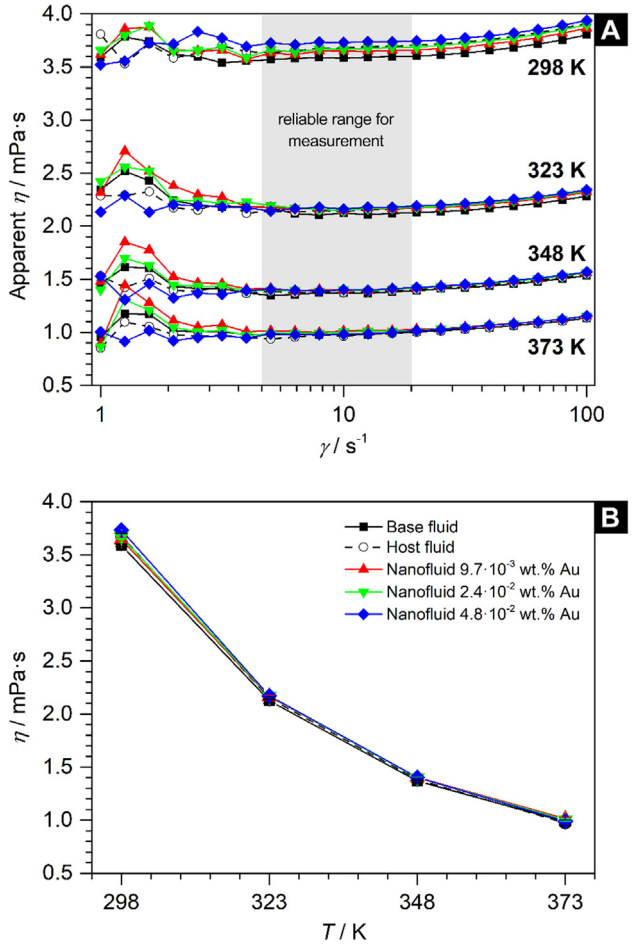

Fig. 4. Dynamic viscosity as a function of the shear rate [A] and temperature [B]. Solid lines do not represent actual data but are included as guide to the eye. Data is available in Supplementary Material.

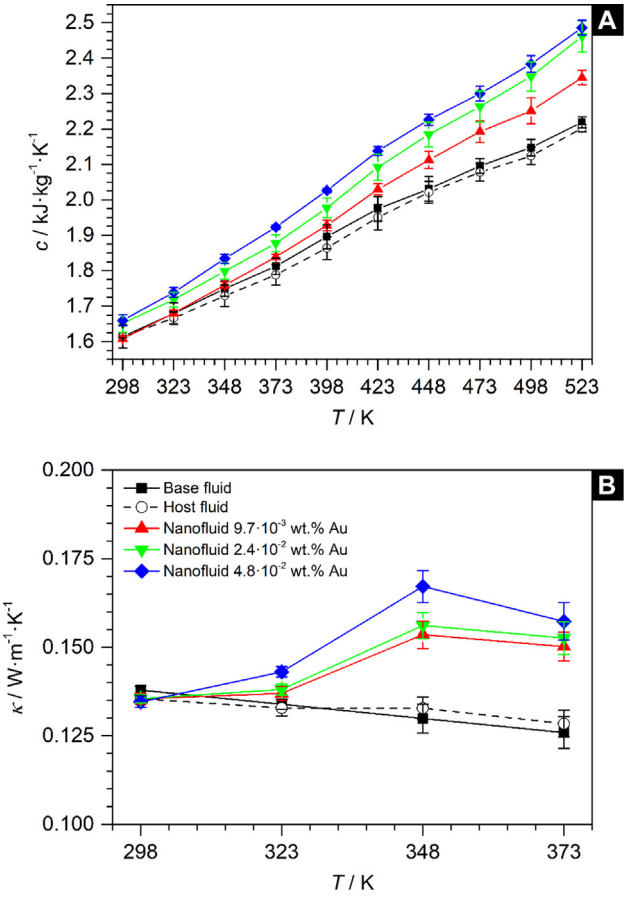

Fig. 5. Specific heat [A] and thermal conductivity [B] as a function of temperature. Solid lines do not represent actual data but are included as guide to the eye. Data is available in Supplementary Material.

the same Newtonian flow behaviour of the base fluid, but the addition of Au nanoplates causes a non-marginal change in viscosity, with relative increments of 1.6 ± 0.5 %, 2.3 ± 0.5 % and 4.0 ± 0.4 % at 298 K (differences become negligible at higher temperatures) for mass fractions of $9.7{\cdot}10^{-3}$ wt%, $2.4{\cdot}10^{-2}$ wt% and $4.8{\cdot}10^{-2}$ wt%, respectively. Although non-marginal, these increments are sufficiently small to safely conclude that any potential gains in specific heat or thermal conductivity will not be counterbalanced by viscosity, at least at high temperatures, which is a result of great significance.

Specific heat – The energy storage capacity is now discussed based on the measured specific heat values, which are shown in Fig. 5A, as a function of temperature. The relative standard deviation of the measurements is better than ± 3.5 %. In line with our experimental scheme so far, the measured specific heat values for the base fluid are verified to be in good agreement compared to the reference specific heat values provided by the supplier, with a maximum relative deviation below 1.7 %, and the addition of Triton X-100 (1.0 wt%) is determined not to change specific heat either. The addition of Au nanoplates increases the specific heat of the base fluid, an effect that becomes more significant for increasing temperatures and mass fractions. The relative enhancements are 5.7 ± 1.2 %, 10.9 ± 2.1 % and 12.0 ± 1.2 %, at 523 K (the maximum temperature of operation for the fluid to be in liquid phase at 1013 hPa), for mass fractions of $9.7{\cdot}10^{-3}$ wt%, $2.4{\cdot}10^{-2}$ wt% and $4.8{\cdot}10^{-2}$ wt%, respectively.

For the application, an increase in specific heat means that more energy per unit mass and unit temperature can be directly stored by the fluid, without implicating a secondary medium for energy storage. This increment is rationally associated to strong chemical interactions between base fluid molecules and Au surfaces. It has been previously reported by our group that interactions between species at solid–liquid interfaces play a key role for specific heat enhancements [44,45], and it is known that aromatic species are likely to be coordinated to Au atoms due to charge transfer, dispersion interactions and relativistic effects [46].

Thermal conductivity – The measured thermal conductivity values are presented in Fig. 5B, also as a function of temperature. The relative standard deviation of the measurements is better than 3.2 %. In the absence of a liquid-phase primary reference standard, the base fluid was used as a reference to correct deviations in the measurement of the apparent thermal conductivity due to natural convection. As for all the previously presented properties, the addition of Triton X-100 (1.0 wt%) is determined not to change thermal conductivity. In contrast, the addition of Au nanoplates increases thermal conductivity, with respect to the base fluid, by 19.3 ± 5.3 %, 21.2 ± 5.7 % and 24.9 ± 6.1 % at 373 K, for mass fractions of $9.7{\cdot}10^{-3}$ wt%, $2.4{\cdot}10^{-2}$ wt% and $4.8{\cdot}10^{-2}$ wt%, respectively. The THB technique does not seem to have enough resolution to precisely determine the differences in thermal conductivity between nanofluid samples in the very diluted regime we are working at, but an enhancement in this property is determined with confidence.

This finding boosts the added value of these nanofluids as heat transfer fluids, as an increase in thermal conductivity is directly translated into higher rates for heat transfer to another medium. Thermal conductivity represents the dominant factor for performance as heat transfer fluids in most figures-of-merit related to energy conversion, and for that it is the most studied property of nanofluids. Increasing thermal conductivity upon addition of Au nanoplates, even in low mass fractions, is consistent with the fact that the thermal conductivity of Au (and solids in general) is much higher than that of this base fluid. However, the addition of Au nanoplates also affects the behaviour for increasing temperatures, even though the base fluid is still the majority component, as it was previously observed with Pd nanoplates in the exact same base fluid [47].

3.4. Performance of Au nanoplate-containing nanofluids as working fluids for CSP systems

To round off the central discussion about the applicability of the previously characterised samples, an assessment of their performance as HTFs for CSP-PTC plants is presented. The use of a convenient FoM (*i.e.*, a rationalised combination of a set of key physical properties for a given application) is a trivial procedure to compare the convective heat transfer coefficient, h, of different fluids in a given system. Lenert et al. [32] discussed about this topic with relation to solar-to-thermal energy conversion applications, and provided a particular case of the Mouromtseff number, Mo, given by.

$$h \propto Mo = \rho^{2.0} \cdot \eta^{-1.4} \cdot c^{1.6} \cdot \kappa^{1.8} \tag{1}$$

in which the powers have been parametrised around the boundary conditions defined by an absorbing tube in the focal line of a PTC, under uniform irradiated heat flux and forced turbulent convection. Here, we will use the following ratio as a FoM.

$$\mathrm{FoM} = \frac{h_{\mathrm{nf}}}{h_{\mathrm{bf}}} \propto \frac{Mo_{\mathrm{nf}}}{Mo_{\mathrm{bf}}} = \left(\frac{\rho_{\mathrm{nf}}}{\rho_{\mathrm{bf}}}\right)^{2.0} \cdot \left(\frac{\eta_{\mathrm{nf}}}{\eta_{\mathrm{bf}}}\right)^{-1.4} \cdot \left(\frac{c_{\mathrm{nf}}}{c_{\mathrm{bf}}}\right)^{1.6} \cdot \left(\frac{\kappa_{\mathrm{nf}}}{\kappa_{\mathrm{bf}}}\right)^{1.8} \tag{2}$$

where the bf and nf subscripts stand for base fluid and nanofluid, respectively. The values for this FoM are presented in Fig. 6, as a function of temperature. The FoM > 1.0 condition implies that the nanofluid enhances the heat transfer with respect to the base fluid, which is satisfied for temperatures above 323 K. Rheological penalty domains heat transfer for temperatures below that. Maximum enhancement in convection heat transfer performance within the range of temperatures and mass fractions under study is found to be 63 % for an Au nanoplate content of $4.8{\cdot}10^{-2}$ wt% at 373 K, whereas the addition of the Triton X-100 surfactant is again verified not to have a significant impact for heat transfer.

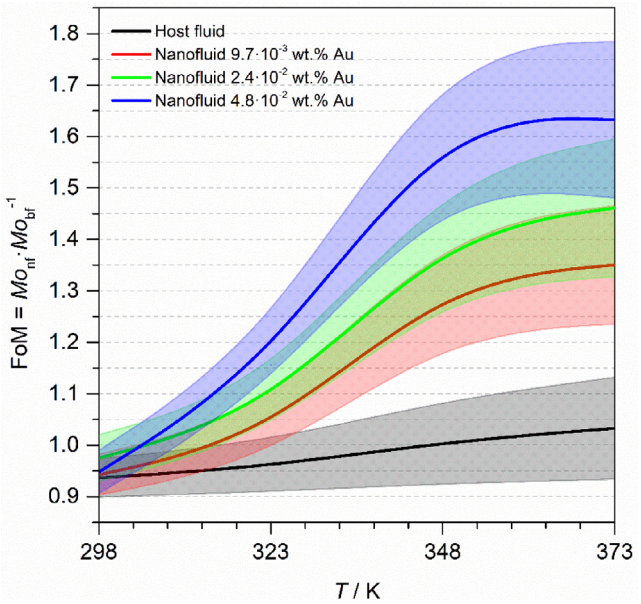

Fig. 6. Figure-of-merit for all heat transfer nanofluids under study, compared to the base fluid, as a function of temperature. Solid lines are B-splined functions fitted to experimental data. Coloured regions show the data deviation, which were estimated using the quadratic approximation.

The FoM analysis makes easy to identify these nanofluids with Au nanoplates better candidates than the standard Dowtherm A fluid to be used as HTF in CSP-PTC plants. However, it provides no immediate information about the consequences of their use for the design requirements, if any, or the efficiency improvement of these plants. Such discussion requires (i) a realistic estimation of the array length and thermal efficiency of PTCs, (ii) the effectiveness of a coupled heat exchanger for steam generation, and (iii) the overall CSP system efficiency, using these nanofluids as HTFs under actual operation conditions. For the first part we have used a minimally simplified, approximate analytic solution developed by Bellos et al. [33] for steady state surface-absorber PTC, also under uniform irradiated heat flux and forced turbulent convection. For the second part we have used the number of transfer units (NTU) method. The overall CSP system performance, Ψ_{CSP}, is simply calculated as.

$$\Psi_{\mathrm{CSP}} = \Psi_{\mathrm{PTC}} \cdot \Psi_{\mathrm{HEx}} \tag{3}$$

where Ψ_{PTC} and Ψ_{HEx} are the parabolic-trough collector efficiency and heat exchanger effectiveness. All formulas for this assessment and their parameters, including their actual values in SI units, are included in the Supplementary Material. The necessary values of density, dynamic viscosity, specific heat and thermal conductivity at high operating temperatures were extrapolated from best fitting functions to the experimental data obtained in this work.

Fig. 7A shows the outlet temperature, T_{out}, as a function of the total length of the array of PTCs, L, using either the Dowtherm A (which is the actual working fluid for this application, and the base fluid of choice for this work) or any of the Au nanoplate-containing nanofluids as HTFs. The incident radiative heat flux, the width of the collector aperture, the efficiency of optical elements, pipe diameters and flow rates are the same in all cases. The inlet temperature, T_{in} = 473 K, is also the same in all cases. The upper limit for the range of temperatures of interest is T_{max} = 673 K, which is the maximum operating temperature for Dowtherm A stability not to be compromised. We know from Fig. 7A that the $T_{\mathrm{out}} = T_{\mathrm{max}}$ condition should be fulfilled at $L \simeq 250$ m with the typ-

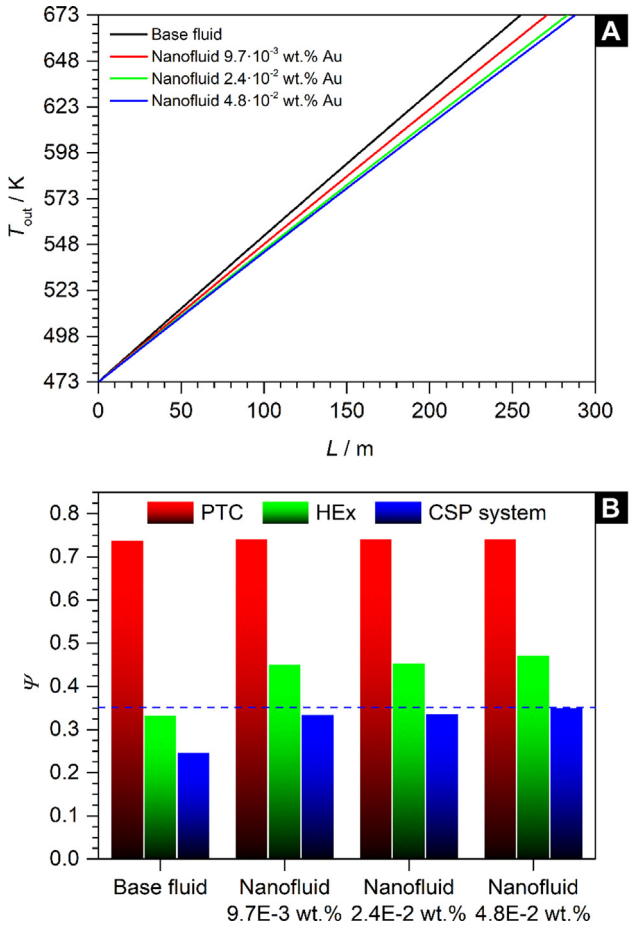

Fig. 7. Estimated outlet temperatures as a function of the length of the PTC array, *L*, [A] and collector thermal efficiency, heat exchanger effectiveness and the overall CSP system performance [B] using different HTFs. The dashed blue line in [B] indicates the maximum performance. (For interpretation of the references to colour in this figure legend, the reader is referred to the web version of this article.)

ical Dowtherm A HTF, and at $L \simeq 270$–290 m with the nanofluids as HTF, depending on the mass fraction of Au nanoplates. Due to their higher specific heat, a longer PTC array is needed for nanofluids to be heated up to 673 K. That does not necessarily imply that the efficiency of the collector, Ψ_{PTC}, becomes lower. In fact, it seems to be invariant, according to Fig. 7B. In contrast, the effectiveness of the coupled heat exchanger, Ψ_{HEx}, is estimated to increase up to 45–47 % using these Au nanoplate-containing nanofluids rather than the Dowtherm A fluid, due to their higher specific heat and thermal conductivity. The overall CSP system performance, Ψ_{CSP}, is predicted to increase from 24.7 % with the typical Dowtherm A fluid up to 35.1 % with the $4.8{\cdot}10^{-2}$ wt% Au nanofluid.

In summary, it seems possible to increase the solar-to-thermal energy conversion efficiency in CSP systems by 8.9–10.3 % by adding Au nanoplates in mass fractions in the order of magnitude of 10^{-2} wt% to improve its specific heat and thermal conductivity, with no prohibitive practical implications arising from the use of the nanomaterial. Au nanoplates are prepared following a straightforward, easily scalable chemical synthesis procedure. No sedimentation and clogging are expected because these nanofluids exhibit long-term stability. No additional pumping power is required as the density and dynamic viscosity of these nanofluids is very much the same than those of the base fluid. Only because of the increase in specific heat, the total length of the PTC array in the solar field by 20–40 m for the HTF to achieve its maximum operating temperature. This, together with the addition of Au nanoplates in the above stated concentrations, represents a negligible cost to the overall installation cost of a plant of this kind, so it is safe to assume that the use of these nanofluids can improve the efficiency of CSP-PTC systems at virtually no additional cost.

4. Conclusions

We have presented a laboratory-to-industry study on heat transfer nanofluids for next-generation CSP plants. It has been experimentally proven that the addition of a small mass fraction of Au nanoplates, in the order of 10^{-2} wt%, is sufficient to induce a quantitatively meaningful change in the thermophysical properties of the conventional HTF of this application (the eutectic and azeotropic mixture of DPO and BP). For instance, with a $4.8{\cdot}10^{-2}$ wt% of Au nanoplates, specific heat increases by 12.0 ± 1.2 % at 523 K and thermal conductivity increases by 24.9 ± 6.1 % at 373 K, with no rheological penalty. The key set of physical properties that has been characterised allowed us to make a realistic estimation of the performance of a prototypical CSP plant using these heat transfer nanofluids. We determined that the so-called performance increases up to 35.1 % with previously mentioned sample, compared to the predicted 24.7 % with the conventional HTF. This enhancement comes with no economically prohibitive structural changes to existing installations. Such result is not only of technological relevance but also of social significance. For a 100 MW CSP plant like *Valle 1&2* in San José del Valle (Cádiz, Spain), which supplies electricity for 80,000 households, such improvement in performance implies access to reliable, renewable electricity for 8,200 more.

Future research direction on nanofluids for heat transfer applications should aim for a path from laboratory to industrial scale, by undertaking a systematic characterisation of their physical properties and evaluating their performance in the application, for a better development of this new product of nanotechnology and progression towards their maximum potential for heat transfer and thermal management applications in the context a climate crisis in which energy optimisation is a priority goal.

Data availability

All data is available for the readership upon reasonable request.

CRediT authorship contribution statement

Iván Carrillo-Berdugo: Conceptualization, Methodology, Investigation, Formal analysis, Writing – original draft, Visualization, Supervision. **Javier Sampalo-Guzmán:** Investigation. **Juan Jesús Gallardo:** Investigation. **Alejandro Domínguez-Núñez:** Investigation. **Teresa Aguilar:** Formal analysis. **Paloma Martínez-Merino:** Formal analysis. **Javier Navas:** Writing – review & editing, Supervision, Project administration, Funding acquisition.

Data availability

Data will be made available on request.

Declaration of Competing Interest

The authors declare that they have no known competing financial interests or personal relationships that could have appeared to influence the work reported in this paper.

Acknowledgments

I.C.-B. thanks *Ministerio de Universidades del Gobierno de España* for endorsing his postdoctoral position at the University of Cadiz with a *Margarita Salas* fellowship, granted within the call for *Recualificación del Sistema Universitario Español para 2021-2023*, funded by the NextGeneration EU programme of the European Union. The group acknowledges *Ministerio de Ciencia e Innovación del Gobierno de España* (grants RTI2018-096393-B-I00 and UNCA15-CE-2945). This research was also funded by the Andalucía ERDF Operational Programme 2014-2020, managed by *Consejería de Transformación Económica, Industria, Conocimiento y Universidades de la Junta de Andalucía* (grant FEDER-UCA18-107510). Lab diagrams in Fig. 1 were created with the online editor Chemix (https://chemix.org), using I.C.-B.'s 'Boost' subscription, which grants permission for publishing and commercial use. A previous version of the submitted manuscript for this work is available as a preprint at the SSRN repository (doi: 10.2139/ssrn.4119335).

Appendix A. Supplementary material

Supplementary data to this article can be found online at https://doi.org/10.1016/j.molliq.2023.121415.

References

[1] E. Comission, EU Energy in Figures - Statistical Pocketbook 2020 and Country Datasheets, Publications Office of the European Union, 2020.
[2] F. Martins, C. Felgueiras, M. Smitková, Fossil fuel energy consumption in European countries, Energy Proced. 153 (2018) 107, https://doi.org/10.1016/j.egypro.2018.10.050.
[3] D. Enescu, G. Chicco, R. Porumb, G. Seritan, Thermal Energy Storage for Grid Applications: Current Status and Emerging Trends, Energies 13 (2020), https://doi.org/10.3390/en13020340.
[4] J. Lilliestam, T. Barradi, N. Caldés, M. Gomez, S. Hanger, J. Kern, N. Komendantova, M. Mehos, W.M. Hong, Z. Wang, A. Patt, Policies to Keep and Expand the Option of Concentrating Solar Power for Dispatchable Renewable Electricity, Energy Pol. 116 (2018) 193, https://doi.org/10.1016/j.enpol.2018.02.014.
[5] S.A. Kalogirou, Solar Thermal Collectors and Applications, Prog. Energy Combust. Sci. 30 (2004) 231, https://doi.org/10.1016/j.pecs.2004.02.001.
[6] G. Morin, J. Dersch, W. Platzer, M. Eck, A. Häberle, Comparison of Linear Fresnel and Parabolic Trough Collector Power Plants, Sol. Energy 86 (2012) 1, https://doi.org/10.1016/j.solener.2011.06.020.
[7] S.U.S. Choi, J.A. Eastman. Enhancing Thermal Conductivity of Fluids with Nanoparticles, in ASME 1995 International Mechanical Engineering Congress & Exposition (California, USA, 1995), 99-106.
[8] S.U. Ilyas, R. Pendyala, M. Narahari, Stability and thermal analysis of MWCNT-thermal oil-based nanofluids, Colloids Surf., A 527 (2017) 11, https://doi.org/10.1016/j.colsurfa.2017.05.004.
[9] T. Aguilar, I. Carrillo-Berdugo, R. Gómez-Villarejo, J.J. Gallardo, P. Martínez-Merino, J.C. Piñero, R. Alcántara, C. Fernández-Lorenzo, J. Navas, A Solvothermal Synthesis of TiO2 Nanoparticles in a Non-Polar Medium to Prepare Highly Stable Nanofluids with Improved Thermal Properties, Nanomaterials 8, 816, 1 (2020), https://doi.org/10.3390/nano8100816.
[10] T.T. Baby, S. Ramaprabhu, Synthesis and Nanofluid Application of Silver Nanoparticles Decorated Graphene, J. Mater. Chem. 21 (2011) 9702, https://doi.org/10.1039/C0JM04106H.
[11] L.S. Sundar, M.K. Singh, E.V. Ramana, B. Singh, J. Grácio, A.C.M. Sousa, Enhanced Thermal Conductivity and Viscosity of Nanodiamond-Nickel Nanocomposite Nanofluids, Sci. Rep. 4 (2014) 4039, https://doi.org/10.1038/srep04039.
[12] R. Gómez-Villarejo, E.I. Martín, J. Navas, A. Sánchez-Coronilla, T. Aguilar, J.J. Gallardo, R. Alcántara, D. De los Santos, I. Carrillo-Berdugo, C. Fernández-Lorenzo. Ag-based Nanofluidic System to Enhance Heat Transfer Fluids for Concentrating Solar Power: Nano-level Insights, Appl. Energy 194, 19 (2017). https://doi.org/10.1016/j.apenergy.2017.03.003.
[13] R. Gómez-Villarejo, J. Navas, E.I. Martín, A. Sánchez-Coronilla, T. Aguilar, J.J. Gallardo, D. De los Santos, R. Alcántara, C. Fernández-Lorenzo, J. Martín-Calleja. Preparation of Au Nanoparticles in a Non-polar Medium: Obtaining High-efficiency Nanofluids for Concentrating Solar Power. An Experimental and Theoretical Perspective, J. Mater. Chem. A 5, 12483 (2017). https://doi.org/10.1039/C7TA00986K.
[14] H. Xu, C. Chang, J. Zhang, J. Xu, H. Chen, H. Guo, B. Fu, C. Song, W. Shang, P. Tao, T. Deng, Transparent Nanofluids with High Thermal Conductivity for Improved Convective Thermal Management of Optoelectronic Devices, Exp. Heat Trans. (2020), https://doi.org/10.1080/08916152.2020.1829749.
[15] E.V. Timofeeva, W. Yu, D.M. France, D. Singh, J.L. Routbort, Nanofluids for Heat Transfer: An Engineering Approach, Nanoscale Res. Lett. 6, 182, 1 (2011), https://doi.org/10.1186/1556-276X-6-182.
[16] R.A. Taylor, P.E. Phelan, T.P. Otanicar, C.A. Walker, M. Nguyen, S. Trimble, R. Prasher, Applicability of Nanofluids in High Flux Solar Collectors, J. Renew. Sustain. Energy 3, 023104, 1 (2011), https://doi.org/10.1063/1.3571565.
[17] H. Tyagi, P. Phelan, R. Prasher, Predicted Efficiency of a Low-temperature Nanofluid-based Direct Absorption Solar Collector, J. Sol. Energy Eng. 131, 041004, 1 (2009), https://doi.org/10.1115/1.3197562.
[18] D. Singh, E.V. Timofeeva, M.R. Moravek, S. Cingarapu, W. Yu, T. Fischer, S. Mathur, Use of Metallic Nanoparticles to Improve the Thermophysical Properties of Organic Heat Transfer Fluids Used in Concentrated Solar Power, Solar Energy 105 (2014) 468, https://doi.org/10.1016/j.solener.2014.02.036.
[19] J.E. Juliá Bolívar, R. Cazorla Mondragón, L. Hernández López, R. Martínez Cuenca, S.F. Torro Cueco, L. Cabedo Mas. Heat exchange nanofluid, WO 2015/177392 Al (U.J.I.d. Castelló, Spain, 2015).
[20] J. Navas, P. Martínez-Merino, A. Sánchez-Coronilla, J.J. Gallardo, R. Alcántara, E. I. Martín, J.C. Piñero, J.R. León, T. Aguilar, J. Hidalgo Toledo, C. Fernández-Lorenzo, MoS2 Nanosheets vs. Nanowires: Preparation and a Theoretical Study of Highly Stable and Efficient Nanofluids for Concentrating Solar Power, J. Mater. Chem. A 6 (2018) 14919, https://doi.org/10.1039/C8TA03817A.
[21] M. Teruel, T. Aguilar, P. Martínez-Merino, I. Carrillo-Berdugo, J.J. Gallardo, R. Gómez-Villarejo, R. Alcántara, C. Fernández-Lorenzo, J. Navas. 2D MoSe2-based Nanofluids Prepared by Liquid Phase Exfoliation for Heat Transfer Applications in Concentrating Solar Power, Sol. Energ. Mat. Sol. C. 200, 109972, 1 (2019). https://doi.org/10.1016/j.solmat.2019.109972.
[22] P. Martínez-Merino, S. Midgley, E.I. Martín, P. Estellé, R. Alcántara, A. Sánchez-Coronilla, R. Grau-Crespo, J. Navas, Novel WS2-Based Nanofluids for Concentrating Solar Power: Performance Characterization and Molecular-Level Insights, ACS Appl. Mater. Interfaces 12 (2020) 5793, https://doi.org/10.1021/acsami.9b18868.
[23] P. Martínez-Merino, E. Sani, L. Mercatelli, R. Alcántara, J. Navas, WSe2 Nanosheets Synthesized by a Solvothermal Process as Advanced Nanofluids for Thermal Solar Energy, ACS Sustainable Chem. Eng. 8 (2020) 1627, https://doi.org/10.1021/acssuschemeng.9b06489.
[24] T. Aguilar, J. Navas, A. Sánchez-Coronilla, E.I. Martín, J.J. Gallardo, P. Martínez-Merino, R. Gómez-Villarejo, J.C. Piñero, R. Alcántara, C. Fernández-Lorenzo, Investigation of Enhanced Thermal Properties in NiO-based Nanofluids for Concentrating Solar Power Applications: A Molecular Dynamics and Experimental Analysis, Appl. Energy 211 (2018) 677, https://doi.org/10.1016/j.apenergy.2017.11.069.
[25] R. Gómez-Villarejo, E.I. Martín, A. Sánchez-Coronilla, T. Aguilar, J.J. Gallardo, P. Martínez-Merino, I. Carrillo-Berdugo, R. Alcántara, C. Fernández-Lorenzo, J. Navas, Towards the Improvement of the Global Efficiency of Concentrating Solar Power Plants by Using Pt-based Nanofluids: The Internal Molecular Structure Effect, Appl. Energy 228 (2018) 2262, https://doi.org/10.1016/j.apenergy.2018.07.062.
[26] R. Gómez-Villarejo, P. Estellé, J. Navas, Boron Nitride Nanotubes-based Nanofluids with Enhanced Thermal Properties for Use as Heat Transfer Fluids in Solar Thermal Applications, Sol. Energ. Mat. Sol. C. 205, 110266, 1 (2020), https://doi.org/10.1016/j.solmat.2019.110266.
[27] T. Aguilar, E. Sani, L. Mercatelli, I. Carrillo-Berdugo, E. Torres, J. Navas, Exfoliated Graphene Oxide-based Nanofluids with Enhanced Thermal and Optical Properties for Solar Collectors in Concentrating Solar Power, J. Mol. Liq. 306, 112862, 1 (2020), https://doi.org/10.1016/j.molliq.2020.112862.
[28] M.G. Jeong, J.B. Kim, C. Qin, J. Lee, B.J. Lee, Synthesis of therminol-graphite nanofluids and photo-thermal conversion properties, Int. J. Energ. Res. 45 (2021) 11320, https://doi.org/10.1002/er.6568.
[29] A. Mwesigye, Z. Huan, J.P. Meyer, Thermodynamic optimisation of the performance of a parabolic trough receiver using synthetic oil–Al2O3 nanofluid, Appl. Energ. 156 (2015) 398, https://doi.org/10.1016/j.apenergy.2015.07.035.
[30] A. Mwesigye, Z. Huan, J.P. Meyer, Thermal Performance and Entropy Generation Analysis of a High Concentration Ratio Parabolic Trough Solar Collector with Cu-Therminol®VP-1 Nanofluid, Energy Convers. Manage. 120 (2016) 449, https://doi.org/10.1016/j.enconman.2016.04.106.
[31] A. Mwesigye, I.H. Yilmaz, J.P. Meyer, Numerical Analysis of the Thermal and Thermodynamic Performance of a Parabolic Trough Solar Collector Using SWCNTs-Therminol®VP-1 Nanofluid, Renewable Energy 119 (2018) 844, https://doi.org/10.1016/j.renene.2017.10.047.
[32] A. Lenert, Y. Nam, E.N. Wang, Heat Transfer Fluids, Annu. Rev. Heat Transfer 15 (2012) 93, https://doi.org/10.1615/AnnualRevHeatTransfer.2012004122.
[33] E. Bellos, C. Tzivanidis, Analytical Expression of Parabolic Trough Solar Collector Performance, Designs 2, 9, 1 (2018), https://doi.org/10.3390/designs2010009.
[34] B. Lim, M. Jiang, J. Tao, P.H.C. Camargo, Y. Zhu, Y. Xia, Shape-Controlled Synthesis of Pd Nanocrystals in Aqueous Solutions, Adv. Funct. Mater. 19 (2009) 189, https://doi.org/10.1002/adfm.200801439.
[35] Y. Xiong, I. Washio, J. Chen, H. Cai, Z.-Y. Li, Y. Xia, Poly(vinyl pirrolidone): A Dual Functional Reductant and Stabilizer of the Facile Synthesis of Noble Metal Nanoplates in Aqueous Solutions, Langmuir 22 (2006) 8563, https://doi.org/10.1021/la061323x.
[36] S.S. Shankar, S. Bhargava, M. Sastry, Synthesis of Gold Nanospheres and Nanotriangles by the Turkevich Approach, J. Nanosci. Nanotechnol. 5 (2005) 1721, https://doi.org/10.1166/jnn.2005.192.

[37] W. Yu, S.U.S. Choi, An Effective Thermal Conductivity Model of Nanofluids with a Cubical Arrangement of Spherical Particles, J. Nanosci. Nanotechnol. 5 (2005) 580, https://doi.org/10.1166/jnn.2005.065.
[38] R. Hentschke, On the Specific Heat Capacity Enhancement in Nanofluids, Nanoscale Res. Lett. 11, 88, 1 (2016), https://doi.org/10.1186/s11671-015-1188-5.
[39] A.V. Naumkin, A. Kraut-Vass, S.W. Gaarenstroom, C.J. Powell. NIST X-ray Photoelectron Spectroscopy Database, in NIST Standard Reference Database 20, Version 4.1, (2012). http://doi.org/10.18434/T4T88K.
[40] S.R. Beeram, F.P. Zamborini, Purification of Gold Nanoplates Grown Directly on Surfaces for Enhanced Localized Surface Plasmon Resonance Biosensing, ACS Nano 4 (2010) 3633, https://doi.org/10.1021/nn1007397.
[41] S. Hong, K.L. Shuford, S. Park, Shape Transformation of Gold Nanoplates and their Surface Plasmon Characterization: Triangular to Hexagonal Nanoplates, Chem. Mater. 23 (2011) 2011, https://doi.org/10.1021/cm103273c.
[42] M. Chandrasekar, S. Suresh, T. Senthilkumar, Mechanisms proposed through experimental investigations on thermophysical properties and forced convective heat transfer characteristics of various nanofluids – A review, Renew. Sustain. Energy Rev. 16 (2012) 3917, https://doi.org/10.1016/j.rser.2012.03.013.
[43] M. Laun, D. Auhl, R. Brummer, D.J. Dijkstra, C. Gabriel, M.A. Mangnus, M. Rüllmann, W. Zoetelief, U.A. Handge, Guidelines for checking performance and verifying accuracy of rotational rheometers: viscosity measurements in steady and oscillatory shear (IUPAC Technical Report), Pure Appl. Chem. 86 (2014) 1945, https://doi.org/10.1515/pac-2013-0601.
[44] I. Carrillo-Berdugo, S. Midgley, D. Zorrilla, R. Grau-Crespo, J. Navas, Understanding the Specific Heat Enhancement in Metal-containing Nanofluids for Thermal Energy Storage: Experimental and Ab-initio evidence for a Strong Interfacial Layering Effect, ACS Appl. Energy Mater. 3 (2020) 9246, https://doi.org/10.1021/acsaem.0c01556.
[45] I. Carrillo-Berdugo, R. Grau-Crespo, D. Zorrilla, J. Navas, Interfacial molecular layering enhances specific heat of nanofluids: evidence from molecular dynamics, J. Mol. Liq. 325, 115217, 1 (2020), https://doi.org/10.1016/j.molliq.2020.115217.
[46] J. Granatier, P. Lazar, M. Otyepka, P. Hobza, The Nature of the Binding of Au, Ag, and Pd to Benzene, Coronene, and Graphene: From Benchmark CCSD(T) Calculations to Plane-Wave DFT Calculations, J. Chem. Theory Comput. 7 (2011) 3743, https://doi.org/10.1021/ct200625h.
[47] I. Carrillo-Berdugo, P. Estellé, E. Sani, L. Mercatelli, R. Grau-Crespo, D. Zorrilla, J. Navas, Optical and transport properties of metal-oil nanofluids for thermal solar industry: experimental characterization, performance assessment and molecular dynamics insights, ACS Sust. Chem. Eng. 9 (2021) 4194, https://doi.org/10.1021/acssuschemeng.1c00053.